

Far-infrared loops in the 2nd Galactic Quadrant

Cs. Kiss^{1,2}, A. Moór¹, and L. V. Tóth^{2,3}

¹ Konkoly Observatory of the Hungarian Academy of Sciences, P.O. Box 67, H-1525 Budapest, Hungary

² Max-Planck-Institute für Astronomie, Königstuhl 17, D-69117, Heidelberg, Germany

³ Department of Astronomy, Eötvös Lornd University, P.O. Box 32, H-1518 Budapest, Hungary

Received / Accepted ...

Abstract. We present the results of an investigation of the large scale structure of the diffuse interstellar medium in the 2nd Galactic Quadrant ($90^\circ \leq l \leq 180^\circ$). 145 loops were identified on IRAS based far-infrared maps. Our catalogue lists their basic physical properties. The distribution clearly suggests that there is an efficient process that can generate loop-like features at high galactic latitudes. Distances are provided for 30 loops. We also give an observational estimate on the volume filling factor of the hot gas in the Local Arm, $4.6\% \leq f_{2nd} < 6.4\%$.

Key words. Catalogs – ISM: bubbles – Galaxy: structure

1. Introduction

A study of the diffuse interstellar medium is presented, a step in the way deriving the near-past and near-future of the galactic star formation. The large scale structure of the ISM in the Galaxy is diverse with the complex distribution of cavities, filaments, arc, loops and shells, which is often referred to as the “Cosmic Bubble Bath” (Brand & Zealey, 1975). Ridges of enhanced radio continuum emission extending to high galactic latitudes have been known since the 60s. The first extensively studied examples are Loop I (Large et al., 1966), Loop II (“Cetus Arc” Large et al., 1962) and Loop III (Large et al., 1962). Later anomalous HI features like worms, chimneys, supershells were identified and catalogued, up to a characteristic size of ~ 2 kpc with expansion velocities of ~ 20 km s⁻¹ (Heiles, 1979, 1980, 1984; Hu, 1981; Koo & Heiles, 1991). These were associated with voids in the HI distribution (see e.g. Palouš, 1996, for a review). Similar complex morphology has been recognized in some nearby spiral and irregular galaxies e.g. M 31 (Brinks, 1981), M 33 (Deul & den Hartog, 1990) and the Magellanic Clouds (Staveley-Smith et al., 1992; Kim et al., 1998).

The most studied galactic shells were formed by supernova (SN) explosions and winds of massive stars (Tenorio-Tagle & Bodenheimer, 1988). However, high velocity clouds (HVCs) may also form large cavities when infalling from the galactic halo and colliding with the ISM of the disc. A remarkable example of a HVC – galactic disc interaction is the North Celestial Pole (NCP) loop (Meyerdierks et al., 1991). Ehlerová & Palouš (1996) investigated the origin of galactic HI shells and found, that those are likely related to star for-

mation, and not to the infall of HVCs. Apart from the connection of these features to young massive stars and their associations, they may also provide a nest for the next generation of stars via the process of propagating star formation. The idea was first proposed by Oort (1954) and Öpik (1953), and later followed by observational evidences (see Blaauw, 1991, for a review). This mechanism was modelled in detail by Elmegreen & Lada (1977) and successfully applied to the sequential formation of subgroups in OB associations. Gamma ray bursts may also be responsible for the formation of the largest HI holes, as proposed by Efremov et al. (1998) and Loeb & Perna (1998). Nonlinear development of instabilities in the ISM may form large cavities as well, without stellar energy injection (Wada et al., 2000; Korpi et al., 1999; Klessen et al., 2000; Sánchez-Salcedo, 2001).

The cavities of the ISM contain low density hot gas in the multiphase model by McKee & Ostriker (1977). The filling factor f of this hot gas in the galactic disc is an important parameter of the ISM, which is poorly constrained observationally. Ferrière (1998) and Gazol-Patiño & Passot (1999) estimate $f \approx 20\%$ at the solar circle, which drops to $f = 3-8\%$ for $8.5 \leq R_\odot \leq 10$ kpc galactocentric distances.

The 21 cm emission of diffuse HI clouds is well-correlated with the $100\mu\text{m}$ FIR emission (Boulanger & Péroult, 1988). This extended emission is often referred to as the galactic cirrus (Low et al., 1984). A typical far-infrared colour of $\Delta I_{60}/\Delta I_{100} = 0.25$ was derived from IRAS/ISSA maps when the gains are corrected according to Wheelock et al. (1994). According to COBE/DIRBE results its dust colour temperature is $T_d \approx 18$ K (Lagache et al., 1998).

Studies of the large scale structure of the cirrus emission and loop- or arc-like features were restricted so far to

low galactic latitudes in the far-infrared (Schwartz, 1987; Marston, 1996), and reached only medium galactic latitudes in radio surveys. Detailed investigations of individual loops were performed only in the vicinity of the galactic plane. Recently Daigle et al. (2003) presented the first automatic tool for detecting expanding HI shells using artificial neural networks. Their data is restricted to the sky area $75^\circ \leq l \leq 145^\circ$ and $-3^\circ \leq b \leq 5^\circ$ and their detection strategy is based on the velocity information of the HI data rather than morphology.

In order to get a complete, full-scale view on the large-scale structure of the cold diffuse ISM, in our study we searched the whole 2nd galactic quadrant ($90^\circ \leq l \leq 180^\circ$; $-90^\circ \leq b \leq 90^\circ$) for intensity enhancements in the interstellar medium, showing loop-like structures.

2. Data analysis

2.1. Quest for loops on far-infrared maps

We investigated the 60 and 100 μm ISSA plates (IRAS Sky Survey Atlas, Wheelock et al., 1994) in order to explore the distribution of dust emission in the 2nd Galactic Quadrant. We created composite images of the 12.5×12.5 sized individual ISSA plates using the "geom" and "mosaic" procedures of the IPAC-Skyview package, both at 60 and 100 μm . These images were built up typically from ~ 10 -15 ISSA plates, reaching a size of $\sim 40^\circ \times 40^\circ$. Loop-like intensity enhancements were searched by eye on the 100 μm mosaic maps. Loops by our definition must show an excess FIR intensity confined to an arc-like feature, at least 60% of a complete ellipse-shaped ring. A loop may consist of a set of bright, more or less isolated, extended spots, or may be a diffuse ring or part of a ring. The size of the mosaic image limits the maximal size of the objects found. On the other hand, due to the relatively large size of the investigated regions, loop-like intensity enhancements with a size of $\leq 1^\circ$ were not searched. The original ISSA I_{60}^{ISSA} and I_{100}^{ISSA} surface brightness values were transformed to the COBE/DIRBE photometric system, using the conversion coefficients provided by Wheelock et al. (1994):

$$\begin{aligned} - I_{60} &= 0.87 \times I_{60}^{\text{ISSA}} + 0.13 \text{ MJysr}^{-1} \\ - I_{100} &= 0.72 \times I_{100}^{\text{ISSA}} - 1.47 \text{ MJysr}^{-1} \end{aligned}$$

Dust IR emission maps by Schlegel et al. (1998) (SFD) were investigated to derive parameters describing our loop features (see Sect. 2.2). The main differences of the SFD 100 μm map compared to the ISSA maps are the following:

- (1) Fourier-destripping was applied,
- (2) asteroids and non-Gaussian noise were removed,
- (3) IRAS and DIRBE 100 μm maps were combined, preserving the DIRBE zero point and calibration,
- (4) stars and galaxies were removed.

We analysed the radial surface brightness profiles of the loops on the SFD 100 μm map in order to check the effect of the removal of the sources mentioned above. We also used the SFD E(B - V) maps derived from the dust column density maps. In the case of these maps the colour temperature was derived

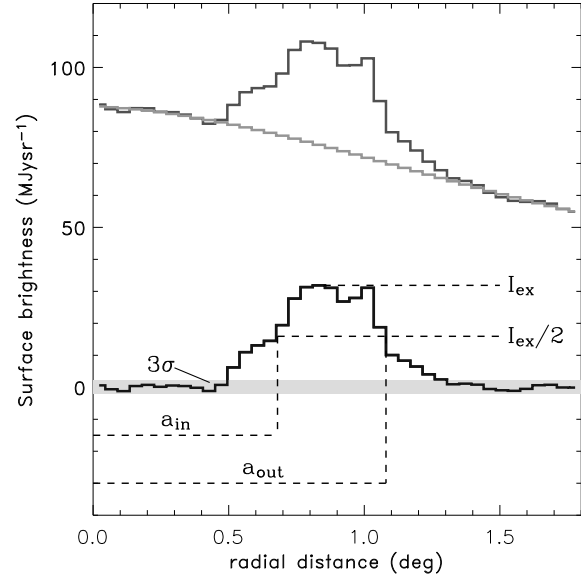


Fig. 1. Intensity profile before (top) and after (bottom) background removal (gray solid line) with the main derived parameters (I_{ex} , σ_{ex} , a_{in} , a_{out} , see Sect. 2.2)

from the DIRBE 100 and 240 μm maps, and a temperature corrected map was used to convert the 100 μm cirrus map to a map proportional to dust column density.

Shape: We approximated the shape of a possible loop by an ellipse, which was then fitted using a 2D least-square fit method. An ellipse shape is expected from SN or stellar wind shells, since (1) non-spherical explosion (wind) may occur, in the most extreme case creating a ring, rather than a shell, and (2) originally spherical shells are distorted to ellipsoidal (i) due to the shear in the direction of galactic rotation (Palouš et al., 1990) and (ii) due to the vertical gravitational field in the galactic disc (see e.g. Ehlerová & Palouš, 1996).

The fitted ellipse is defined with the central (galactic) coordinates, the minor and major semi-axis of the ellipse, and the position angle of the major axis to the circle of galactic latitude at the centre of the ellipse. This latter was defined to be '+' from East to North (or counter-clockwise).

Intensity profile: For all of our loops we extracted radially averaged surface brightness profiles, extended to a distance of twice the major (and minor) axis of the fitted ellipse, using 40 concentric ellipsoidal rings. These surface-brightness profiles (ISSA 100 and 60 μm , SFD 100 μm and SFD reddening maps) were used in the following to determine the basic parameters of the FIR emission in the loop. An example is shown in Fig. 1

2.2. Derived parameters

Significance: The local background was determined using the 'non-loop' points in the radial surface brightness profiles, fit-

*these images are not included in the
astro-ph
document due to their large size*

*they are available at
<http://astro.elte.hu/CFIRLG>
as jpeg files*

Fig. 2. Examples of loops found in the 2nd Galactic Quadrant. *left:* GIRL G134–28, first described by Heiles (1984) as GS 137–27–17. This supershell is located at a distance at 1.5 kpc and has a size of $\sim 0.41 \times 0.31$ kpc; *right:* GIRL G117+00, supershell around the Cas OB5 association in a distance of 2.5 kpc with a size of $\sim 0.31 \times 0.27$ kpc (Moór & Kiss, 2003).

ting a 3rd order polynomial. This appropriate background was removed from each surface brightness profile points. The intensity excess I_{ex} was derived as the maximum value of this background removed profile. In order to check if this value is above the 'noise', we calculated the standard deviation of the background removed intensity in the 'non-loop' values, σ_{ex} , and defined the significance of the loop as $\Psi = I_{ex}/\sigma_{ex}$. We derived significance parameters on 60 and 100 μm ISSA maps and on the SFD 100 μm point source removed sky brightness and reddening maps. The higher the value of Ψ is the higher the intensity excess of the loop over the background, therefore we use this parameter as a 'quality indicator' in the following.

Relative width: Inner and outer edges of the loop wall along the major axis (a_{in} and a_{out} , respectively) are defined as the radial distance at the full width at half power of the background removed intensity profile, $I_{ex}/2$ (Fig. 1) We distinguish three regions for a specific loop: (1) loop interior ($a < a_{in}$), (2) loop wall ($a_{in} \leq a \leq a_{out}$), (3) outer region ($a > a_{out}$). The relative width of the wall of the fitted ellipse is defined as $W = 1 - a_{in}/a_{out}$.

Colour index: We derived a colour index for our loops $\Delta I_{60}/\Delta I_{100}$, from the radially averaged 60 and 100 μm surface brightness profile. This is defined as the slope of the I_{60} vs. I_{100} scatter plot using the data points of the surface brightness profiles in the positions of the loop wall ($a_{in} \leq a \leq a_{out}$) only.

3. Results

3.1. The catalogue

We identified 145 loops in the 2nd Galactic Quadrant. The parameters of these loops are summarized in Table A.1. We

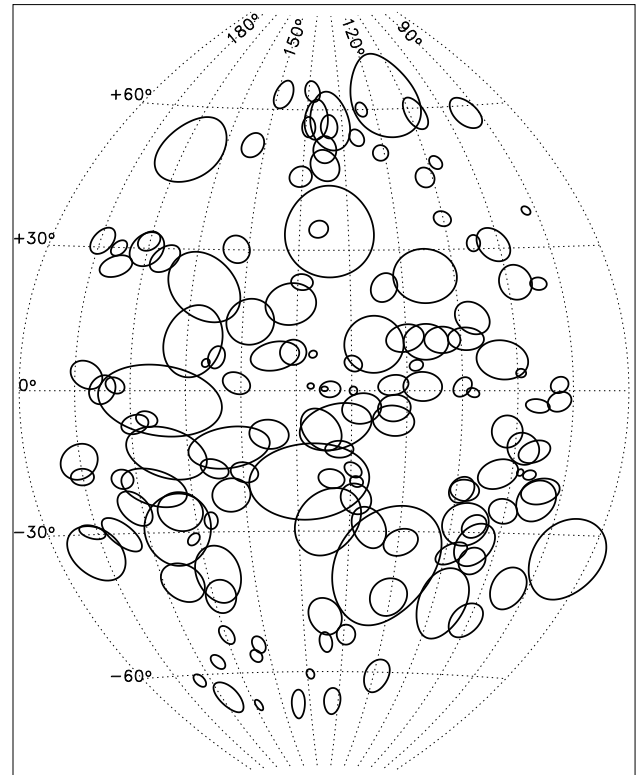


Fig. 3. Distribution of GIRLs in the sky in the 2nd Galactic Quadrant (Aitoff projection), represented by the fitted ellipses

call these objects 'GIRL'-s, abbreviating 'Galactic InfraRed Loops'.

The entries of the catalogue are the following:

- 1.) Name of the loop, derived from the galactic coordinates of the loop centre. The format is : GIRL GLLL \pm BB, the

'GIRL' prefix stands for 'Galactic InfraRed Loops', 'G' marks the galactic coordinate system, 'LLL' is the galactic longitude in degrees, \pm is the sign of the galactic latitude ($+/-$), and 'BB' is the absolute value of the galactic latitude of the loop centre.

- 2.) Central galactic coordinates of the loop (l and b)
- 3.) Semi major and minor axis of the fitted ellipse
- 4.) Position angle of the fitted ellipse. The position angle is defined as '+' from East to North. Zero position angle is pointed to the East in galactic coordinates.
- 5.) Major axes corresponding to the inner and outer edge of the loop wall, derived from the $100\mu\text{m}$ surface brightness profile
- 6.) ISSA 60 and $100\mu\text{m}$, SFD $100\mu\text{m}$ and reddening significance parameters (Ψ_{I60} , Ψ_{I100} , Ψ_{S100} and Ψ_{EBV} , respectively)
- 7.) colour index $\Delta I_{60}/\Delta I_{100}$ of the loop wall

In the electronic version of the catalogue (URL: "http://astro.elte.hu/CFIRLG") we provide the following additional features:

- 8.) $100\mu\text{m}$ ISSA image of the loop with the possible associated objects overlaid
- 9.) ISSA 60 and $100\mu\text{m}$, SFD $100\mu\text{m}$ and SFD E(B-V) surface brightness profiles in FITS format
- 10.) List of objects apparently associated with the loop

An associated object has to be placed in the wall or in the interior of the loop (defined by concentric ellipses, as described above). We considered the following type of possible associated objects (references are indicated)

- dark clouds (Dutra & Bica, 2002)
- supernova remnants (Green, 1994)
- OB-associations (Lang, 1992)
- pulsars (Taylor et al., 1993)
- HII regions (Sharpless, 1959)
- IRAS point source with molecular core FIR colours
- IRAS point source with T Tau star-like FIR colours

Molecular cores and T Tauri stars were selected from the IRAS Point Source Catalogue (Joint IRAS Science Worknig Group, 1988) according to the following criteria:

- point sources associated with galaxies were excluded
- photometric qualities are 2 or better at 12, 25 and $60\mu\text{m}$
- molecular cores:

$$0.4 \leq \log_{10}\left(\frac{F_{25}}{F_{12}}\right) \leq 1.0 \ \& \ 0.4 \leq \log_{10}\left(\frac{F_{60}}{F_{25}}\right) \leq 1.3$$
- T Tauri stars:

$$0.0 \leq \log_{10}\left(\frac{F_{25}}{F_{12}}\right) \leq 0.5 \ \& \ -0.2 \leq \log_{10}\left(\frac{F_{60}}{F_{25}}\right) \leq 0.4$$

following the definitions by Emerson (1998). F_{12} , F_{25} and F_{60} are the 12, 25 and $60\mu\text{m}$ uncorrected IRAS fluxes, respectively.

This list of possible associated object does not take into account the distances of the individual objects, therefore all objects projected to the loop wall or to the interior are included. In the case of a few (30) loops, we were able to derive a distance for the loop based on the distances of associated objects. This is discussed in detail in Sect. 5. The list of associated objects is presented in Appendix C.

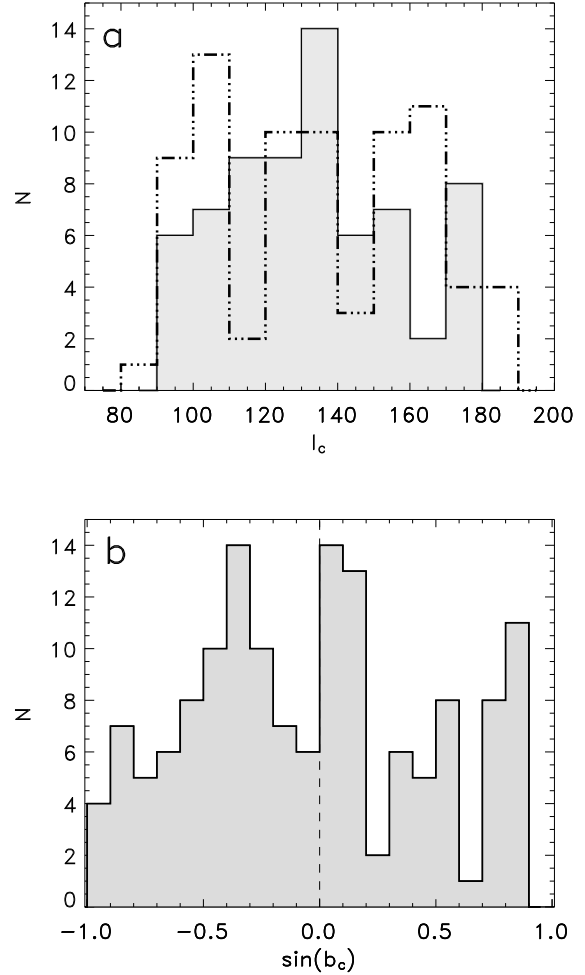


Fig. 4. Distribution of GIRLs in the 2nd Galactic Quadrant. **(a)** Loop-counts vs. galactic longitude. Gray lines with light gray filled area: northern galactic hemisphere ($b > 0^\circ$). Dash-dotted black lines: southern galactic hemisphere ($b < 0^\circ$). **(b)** Loop-counts vs. the 'sin' of the galactic latitude (equal area belts)

3.2. Sky distribution and fundamental statistics

Sky distribution: Fig. 3 presents the distribution of the far-infrared loops found in the 2nd Galactic Quadrant. The distribution of GIRLs seems to be rather complex. However, there are slightly more loops at low ($b \leq 30^\circ$) galactic latitudes than at high ones ($b > 30^\circ$).

It is obvious from Fig 4a that the two galactic hemispheres represent different loop distributions. We have tested the hypothesis that the galactic latitudes of the loop centres on the Northern and Southern hemispheres are drawn from the same distribution. A Kolmogorov–Smirnov test showed that the homogeneous distribution hypothesis could not be accepted at the 80% confidence level. A test performed for the galactic longitude distribution on the two hemispheres (Fig.4b) yielded the same result.

There is a hint in Fig. 3, that most of the loops are part of a structure with scales significantly larger than the individual loop diameters. The most remarkable feature of this kind

is a huge chain of loops seen in the $l \approx 90^\circ\text{--}130^\circ$, $b = -35^\circ\text{--}+5^\circ$ region. In the ranges $l \approx 130^\circ\text{--}140^\circ$, $b \approx +45^\circ\text{--}+65^\circ$ nine loops can be found squeezed to a relatively small area, which correlates well with the position of the Ursa Major molecular complex connected to the expanding shell of the NCP loop (Pound & Goodman, 1997).

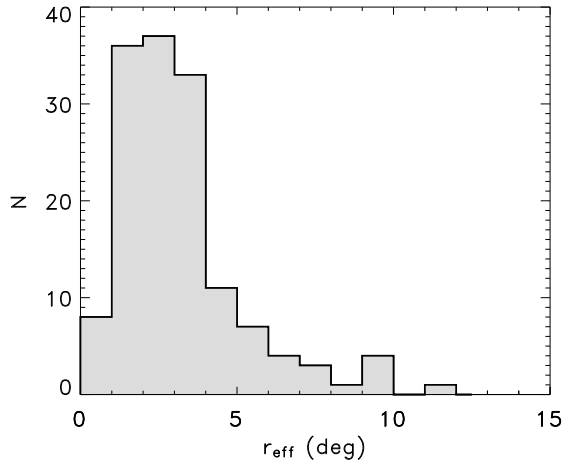


Fig. 5. Apparent size distribution of GIRLs. Size is presented in effective radius, r_{eff} , the geometrical mean of semi-minor and -major axes of the fitted ellipse

Size distribution: We defined the effective radius of our loops as the geometrical mean of the semi-minor and -major axis of the fitted ellipse, $r_{\text{eff}} = \sqrt{a \times b}$. For the whole sample of loops we obtained $m(r_{\text{eff}}) = 3.2$ and $E(r_{\text{eff}}) = 2.7$ for the sample mean and expectation value of the effective radius, respectively.

The size distribution is presented in Fig. 5. Majority (78%) of the loops are in the apparent effective radius $r_{\text{eff}} \leq 4^\circ$, and there are only a few (9) loops $r_{\text{eff}} \geq 7^\circ$. The lower end of the size distribution is limited by our detection method, which excludes features with a size smaller than $\sim 1^\circ$ in diameter.

Distribution of relative width: Fig. 6 shows a Gaussian-like distribution, with an average value of $\langle W \rangle = 0.29$ and a $\text{FWHM} = 0.04$ for the relative width W of the loop walls.

Axis ratio distribution: As mentioned in Sect. 1, it is widely accepted, that galactic loops – identified in any wavelength range – are 2D projections of 3D cavities in the ISM. We compared the expected distribution of the ratio of minor to major axes of the sky-projection of 2D ring to the distribution of the observed minor to major axes ratios in Fig. 7. 2D rings are assumed to be randomly oriented in ϕ and θ polar angles. This figure clearly shows a significant difference between the two distributions. It is not likely that most of our objects are just the projections of 2D rings.

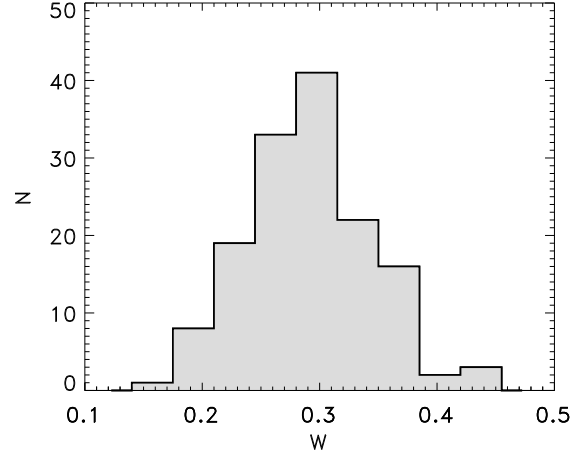


Fig. 6. Distribution of the width of the loop walls relative to the effective radius of the loop ($W = 1 - a_{\text{in}}/a_{\text{out}}$)

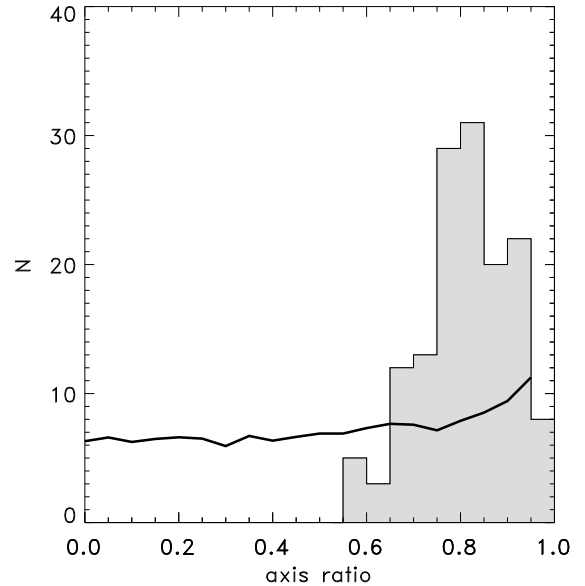


Fig. 7. Comparison of the expected distribution of minor to major axis ratio (assuming randomly oriented 2D rings, solid line) with the distribution of the observed axis ratios (gray histogram).

Significances: In Fig. 9 we compare the significances derived from ISSA $100\mu\text{m}$, ISSA $60\mu\text{m}$, SFD $100\mu\text{m}$ and SFD reddening maps, Ψ_{100} , Ψ_{160} , $\Psi_{\text{SFD}100}$, Ψ_{EBV} (see also Table A.1). The Pearson correlation coefficients are listed in Table 1. The Ψ_{100} , Ψ_{160} , $\Psi_{\text{SFD}100}$ and Ψ_{SFD} significances are well correlated, and in all 145 cases resulted in a definite confirmation of the suspected ellipsoidal structure.

Fig. 8 presents the distribution of ISSA $100\mu\text{m}$ and SFD E(B-V) significances (Ψ_{100} and Ψ_{EBV} , respectively). Based on the definition of Ψ (see Sect 2.2) one can set a limit of $\Psi = 3$ as a value separating *weak* and *prominent* loops (prominent loops are above the “ 3σ ” level of background fluctuations). However,

| correlated significances | correlation coefficients |
|-----------------------------|--------------------------|
| $\Psi_{I100} - \Psi_{I60}$ | 0.77 |
| $\Psi_{I100} - \Psi_{S100}$ | 0.82 |
| $\Psi_{I100} - \Psi_{SEBV}$ | 0.68 |
| $\Psi_{S100} - \Psi_{SEBV}$ | 0.79 |

Table 1. Linear Pearson correlation coefficients of significances derived from ISSA 100 μm (Ψ_{I100}), ISSA 60 μm (Ψ_{I60}), SFD 100 μm (Ψ_{S100}) and SFD E(B-V) (Ψ_{SEBV}) maps.

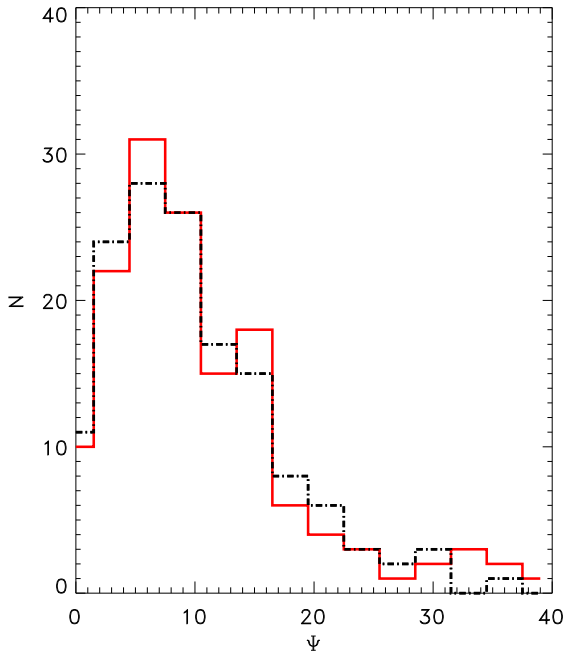


Fig. 8. Distribution of the Ψ_{I100} (gray solid line) and Ψ_{EBV} (black dash-dotted line) significance values

as seen in Fig. 8, the majority of our loops show high sigma values, regardless of the significance type (Ψ_{I100} , Ψ_{I60} , Ψ_{S100} or Ψ_{EBV}) and only very few loops have $\Psi \leq 3$.

Bright fore- or background sources not related to the loop may cause low significances. An example is GIRL G125+09, which has low Ψ_{I100} and Ψ_{S100} (2.4 and 2.6, respectively) but it is outstanding on the reddening maps ($\Psi_{EBV} = 6.0$) and is very conspicuous at 60 μm ($\Psi_{I60} = 17.2$). In addition, this loop is clearly detected in the HI 21 cm line (Kiss et al., 2000). The main reason behind the low significances at 100 μm is the presence of an extremely bright region in the south-eastern part of the loop related to NGC 7822, S 171 and to the Cep OB4 association, which dominates the background of GIRL G125+09.

Far-infrared colour of the loop walls: As seen in Fig. 10 most of the loops have a far-infrared colour similar to that of the extended galactic background emission or galactic cirrus with an average value of $\Delta I_{60}/\Delta I_{100} = 0.25 \pm 0.12$. In the case of a few loops the far-infrared colour significantly deviates from

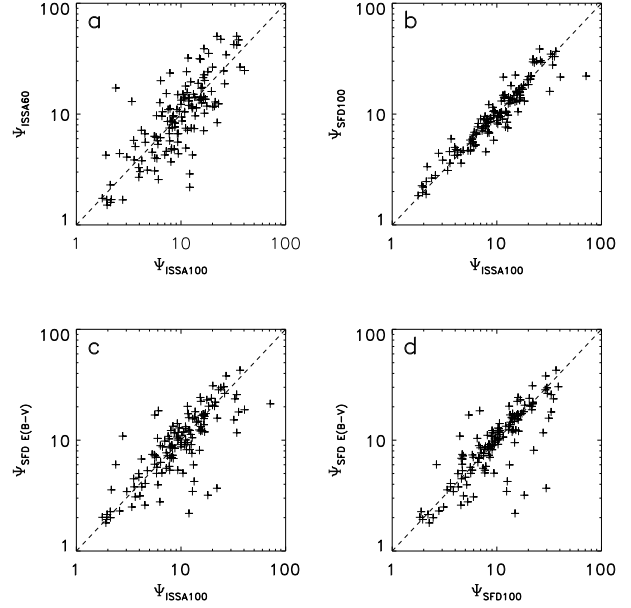


Fig. 9. Comparison of significances extracted from maps of different data sets. (a) ISSA 100 μm vs. ISSA 60 μm ; (b) ISSA 100 μm vs. SFD 100 μm ; (c) ISSA 100 μm vs. SFD reddening maps; (d) SFD 100 μm vs. reddening

that of the extended background, especially in the vicinity of the galactic plane ($|b| \leq 10^\circ$, see Fig. 10), where loops are “warmer” according to their FIR colours. A rather high scatter of FIR colours with high error bars can be observed for the highest galactic latitudes, which could also be related to the less reliable accuracy of the surface brightness calibration in these fields. We conclude that the loops describe the structure of cirrus in the few to $\sim 20^\circ$ scales.

Excess extinction in the loop walls: Using the radially averaged SFD E(B-V) (reddening) profiles extracted from the appropriate maps we estimated the excess visual extinction of the loop walls. Visual extinction values were calculated as $A_V = R \times E(B-V)$, where R is the ratio of total over selective extinction and E(B-V) is the reddening value in a specific sky position. R was chosen to be uniform and set to the standard value of 3.1 of the diffuse medium (Krügel, 2003). The average value of A_V was derived for the inner-, wall- and outer regions (see Sect. 2.2), separately for all loops (A_V^{in} , A_V^{wall} and A_V^{out} , respectively). We also derived an excess visual extinction value for the loop wall, which was defined as

$$\Delta A_V = \frac{2 \cdot A_V^{\text{wall}}}{A_V^{\text{in}} + A_V^{\text{out}}} \quad (1)$$

ΔA_V values show a clear dependence (despite the relatively large scatter around the main trend) on the galactic latitude (Fig. 11a), with values < 0.01 at high galactic latitudes, while reaching $\Delta A_V \approx 10^m$ in the vicinity of the galactic plane.

The relative strength of the excess extinction ΔA_V relative to the background extinction ($A_V^{\text{bg}} = \frac{1}{2}[A_V^{\text{in}} + A_V^{\text{out}}]$) is usually low (in average $\sim 10\%$, as shown in Fig. 11b) except in the case

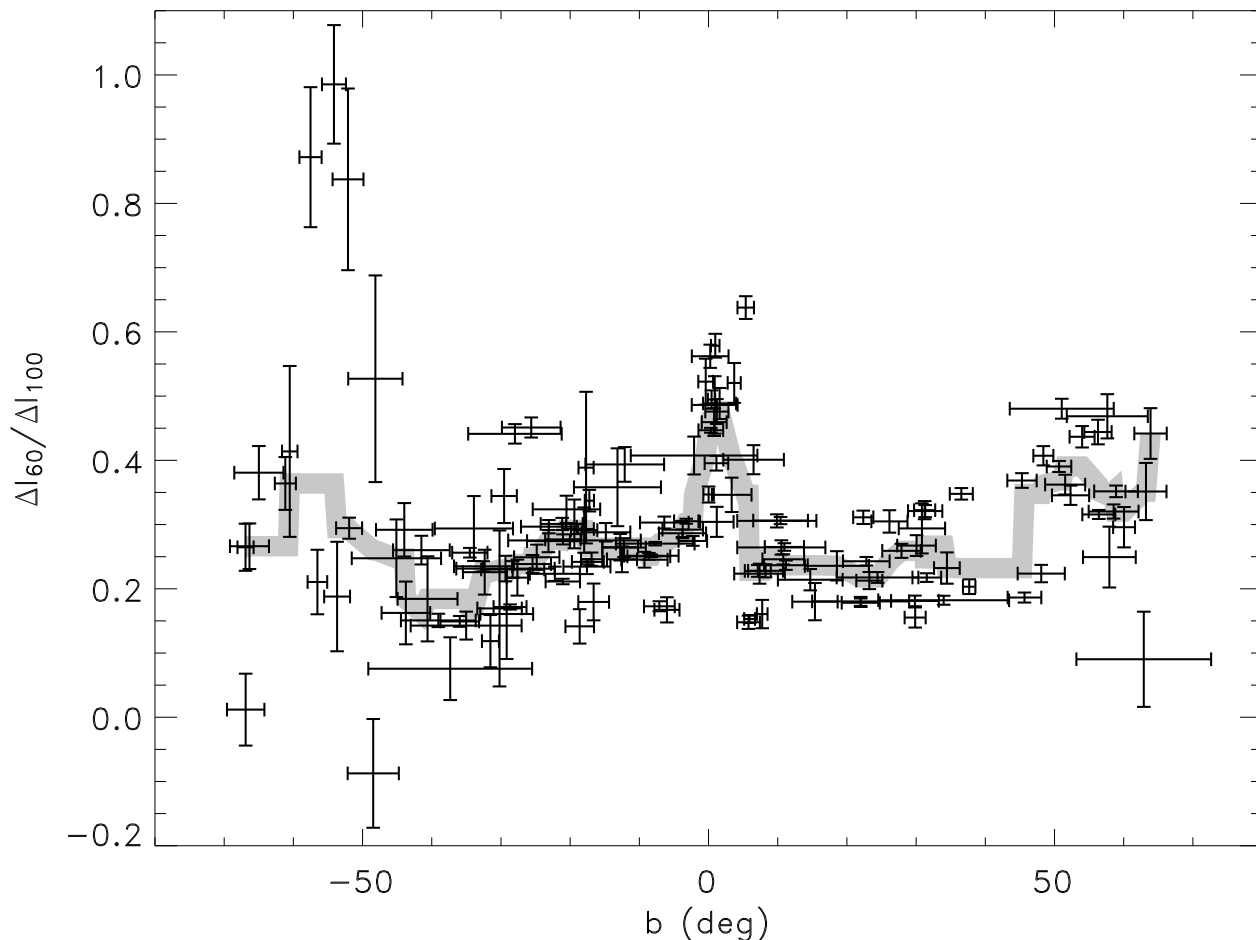


Fig. 10. Distribution of the colour indices of the loop walls ($\Delta I_{60}/\Delta I_{100}$) vs. galactic latitude. Error bars in galactic latitude represent the extension (r_{eff}) of the loop. Error bars of the colour indices are the formal errors of the I_{100} vs. I_{60} scatter plots. The thick gray curve represents the main trend.

of a few loops near the galactic plane. This corresponds to a $\sim 10\%$ increase of column density in the loop walls.

3.3. Distances to individual loops

Derivation of the distance: Many of the major physical properties of a loop (mass, size, particle number density, etc.) can only be tackled if the distance is known. In order to estimate the distance of the loops, we used associated objects with known distances. There are two major classes of these objects: (1) They may be responsible for the formation of the loop itself, or are the remnants of the loop-creating events (we considered pulsars, luminous stars and/or their associations; see Sect. 3.1 for references). (2) They are part of the loop, but identified in another wavelength range (dark clouds and molecular clouds, Dutra & Bica, 2002).

We applied the following main criteria when selecting distance indicators:

- i) Luminous stars had to have the power to form the loop, therefore only O stars and B stars with earlier subtype (or

their associations) were taken into account. The sky position of the stars must be well confined in the central part of the loop (although in some cases fast proper motions might have placed the star far from its original position).

- ii) There must be at least two objects (luminous star, pulsar, dark/molecular cloud) with similar known distances associated with the loop, otherwise the distance hypothesis would be rejected.
- iii) The distances should fit each other within their uncertainties.

Galactic distribution: Based on the distances derived for some of our loops we drew the 3-dimensional distribution of GIRLS with known distances in Fig. 12.

Since our distance indicators are mostly objects which are related to the spiral arms of the Galaxy, the distribution reflects the position of the spiral arms, introducing a selection effect. Loops closer than 800 pc are related to OB associations and luminous stars of the Local Arm and to the nearby interarm region, while another well-defined group can be identified at a

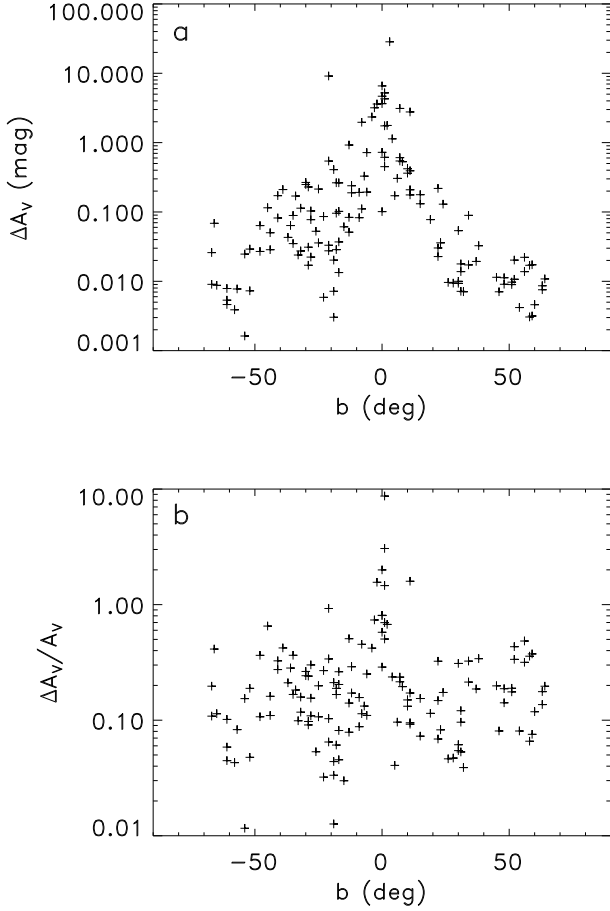


Fig. 11. Excess visual extinction in the loop walls derived from the SFD E(B-V) surface brightness profiles. **(a)** galactic latitude vs. excess visual extinction ΔA_V **(b)** galactic latitude vs. the ratio of the excess visual extinction ΔA_V to the average of the inner and outer visual extinction values ($A_V^{\text{bg}} = \frac{1}{2}[A_V^{\text{in}} + A_V^{\text{out}}]$)

distance of 1.8–2.7 kpc, in agreement with the distance of the Perseus Arm in that direction (Humphreys, 1978). There is a hint that the majority of the GIRLs are within a distance of ~ 800 pc. The most prominent loops remained observable up to a distance of ~ 3 kpc.

4. Discussion

Size distribution: In the Galaxy most of the ISM is confined to a thin disc, forming the Galactic Disc itself (see e.g. Dickey & Lockman, 1990, for a review). Therefore it is expected that any object formed in the ISM should somehow reflect the distribution of the originating medium. Accepting that our loops are features of the cold diffuse ISM, these have been formed in the galactic disc with a scale height of ~ 250 pc. Therefore loops at high galactic latitudes are close to our Solar System. On the other hand, in an exponential disc the number density of the gas and dust is decreasing rapidly with the increasing height from the galactic plane. This allows the gen-

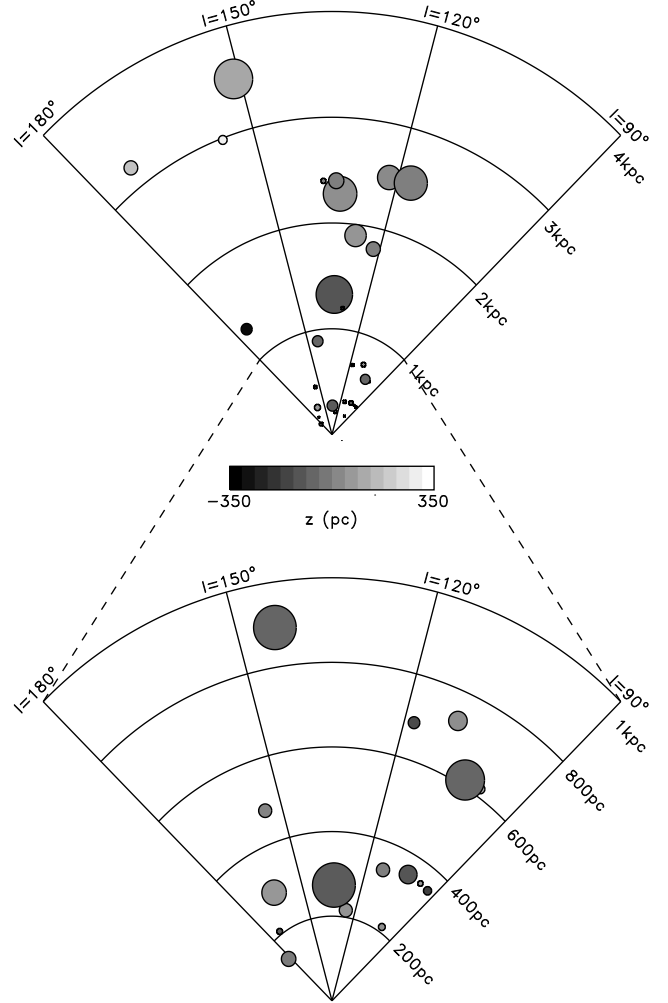


Fig. 12. Loops with known distances in the 2nd Galactic Quadrant, projected to the galactic plane, in cylindrical coordinate system. The top panel shows the loops with projected distances up to 4 kpc. The bottom panel is a magnified view of the region closer than 1 kpc. Different gray tones in both the upper and lower panels code the vertical distance of the loop centres from the galactic plane (see colour bar).

eration of larger SN- or stellar wind bubbles even possessing the same energy input as the ones closer to the galactic plane. Thus one would expect to observe loops with a large apparent size at high galactic latitudes. Still, we found no correlation between the galactic latitude of the loop centres and the effective radii, neither on the northern, nor on the southern galactic hemisphere.

The sky distribution presented in Figs. 3 and 4 shows clearly that the distribution of the GIRLs found at the 2nd Galactic Quadrant is far from that expected e.g. from the exponential disc hypothesis, in which the regions near to the galactic

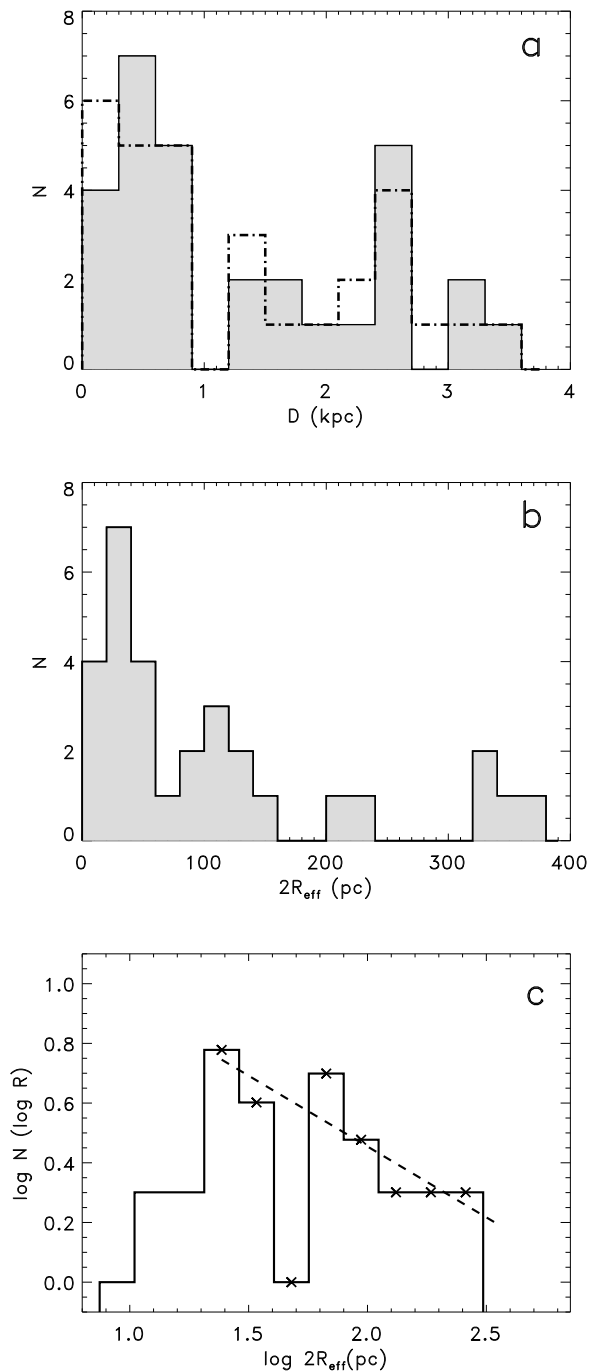


Fig. 13. (a) Distribution of distances among the loops presented in Fig. 12 (solid lines with gray filled area). Dashed-dotted lines represent the distribution of distances *projected* to the galactic plane. (b) Distribution of effective diameters ($2R_{\text{eff}}$) in the same sample. (c) The same as b but displayed and binned on a logarithmic scale. A relation of $\log 2R_{\text{eff}} - \log N$ was fitted for $1.4 \leq 2R_{\text{eff}} \leq 2.6$. The points used for the fit are marked by asterisks (see Sect. 4 for details).

plane should have the largest number of loops and this number should decrease drastically by the increasing galactic latitude. The relatively low number of loops in the galactic midplane

may be explained by multiple overlapping of the loop walls projected on the sky, i.e. many loops might be undiscovered due to confusion. Intervening molecular clouds may also contribute to this confusion.

As discussed in Sect. 3.3, there are two separate distance groups in the known-distance sample. Accepting that the majority of our loop are located in the nearby group (discussed in detail in the next paragraph) at a distance $d \leq 800$ pc, one can obtain the expected ratio of loop counts above and below $|b| = 30^\circ$ for a random distribution with a scale height of $z_H = 250$ pc (Nakanishi & Sofue, 2003). This results in $(N_{\text{low}}/N_{\text{high}})_{\text{calc}} = 2.15$ which should be compared with the observed ratio of $(N_{\text{low}}/N_{\text{high}})_{\text{obs}} = 1.28$ (without the contribution of the Perseus-Arm group). If this discrepancy is caused by confusion as discussed above, we may miss $\sim 40\%$ of the total count in the galactic midplane.

It should be noted that molecular gas extends to galactic latitudes higher (both at the northern (Hartmann et al., 1998, fig. 2) and the southern (Magnani et al., 2000, fig. 1) galactic hemisphere) in the 2nd Galactic Quadrant than in the other parts of the sky. This anomalous feature may also explain the richness of high galactic latitude loops in our sample.

The large number of loops at high galactic latitudes might be a selection effect (loops are easier to be identified due to the lack of confusion). Still, one needs a process that can generate loops far from the galactic plane. One of these processes can be the infall of clouds from the halo, and their collision with the galactic disc. We know some examples, e.g. the NCP-loop (Meyerdierks et al., 1991), but the large number of such loops would require a high rate of cloud infall, which is not supported by observations (Ehlerová & Palouš, 1996).

Another possibility is that turbulent processes in the ISM create ‘loop-like’ structures (Klessen et al., 2000; Korpi et al., 1999; Wada et al., 2000). Nonlinear development of turbulent instabilities may form voids in the ISM without the need of stellar energy injection. These instabilities may be responsible for the large number of loop features at high galactic latitudes since these parts of the sky lack suitable stellar sources (massive O and/or B stars). From the observational point of view the ‘loops’ created by these two different processes are practically indistinguishable, and therefore we are not able to determine the relative importance of these processes.

It is also clear from the figures that local effects play a very important role forming the distribution. We can mention e.g. the high latitude group at $l = 130^\circ - 140^\circ$, $b = 45^\circ - 65^\circ$, which is related to the huge NCP-loop and also belongs to a group of high latitude molecular clouds. Similar groups contribute much to the peaks in Fig. 4a and b, and might be responsible for the deviations from the expected distributions. Since these structures are relatively nearby (e.g. the distance of the NCP-loop is ~ 330 pc), even if we can detect loops up to a distance of ~ 3 kpc, the main contribution comes from loops at small distances (see Sect. 3.3).

In Fig. 13c we displayed the size distribution on a logarithmic scale and fitted the large diameter part (data points marked by asterisks) with a power-law (linear in the log-log plot). Similar investigation has been carried out by Oey & Clarke (1997) for the Small Magellanic Cloud, Holmberg II, M31,

M33 and by Kim et al. (2003) for the HI data of the Large Magellanic Cloud. We found a power law index of $s = -0.47 \pm 0.11$ (following Kim et al., 2003) or $\beta_0 = 1.24 \pm 0.30$ using the transformation by Oey & Clarke (1997), which is lower than that of the other galaxies mentioned above. We note that the distribution has a large scatter and it is better described by a double-peak one than by a power-law.

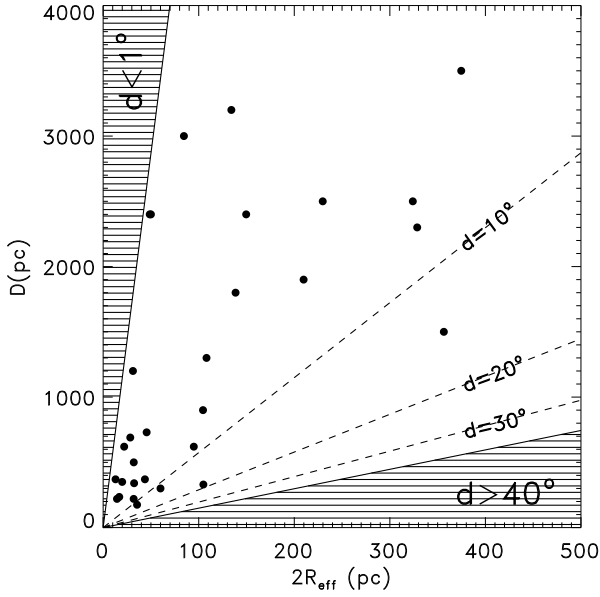


Fig. 14. Relationship between distance and effective diameter ($2R_{eff}$) for loops with known distances (see Table B.1). The shaded areas represent the apparent size limits $2r_{eff} \leq 1^\circ$ and $d \geq 40^\circ$. Due to the limitations discussed in Sect. 2.1 we were not able to detect far-infrared features of these sizes.

Correlation of distance and size: A good correlation can be found between the physical size of the bubble and the derived distance (for the sample in Sect. 3.3) when we derive linear Pearson correlation coefficients for the whole available distance range, up to 3.5 kpc (0.66 and 0.73 for the linear-linear and log-log plot, respectively). Fig. 14 clearly illustrates the limitations of our study: due to the limitations in apparent size ($1^\circ \leq d < 40^\circ$) we identified loops in the allowed region only. This selection effect is more severe for the small-sized part of the distribution ($1^\circ \leq 2r_{eff}$), while even the largest loop is a factor of ~ 2 smaller than the largest detectable feature. The distribution shows two groups, one at $D \leq 800$ pc and one at $D > 800$ pc (Fig. 13a). Within the nearby group practically there is *no correlation* between the distance and physical size (with a linear correlation coefficient of 0.17), therefore this group is not affected by the selection effect. Accordingly, we may derive a statistical result for the local ISM, while the Perseus Arm group is strongly biased. The size distribution of the nearby group lacks the large bubbles ($2R_{eff} > 100$ pc) which are observable in the Perseus-group. The lack of large bubbles in the Local Arm group might be the consequence of a non-continuous star-

formation history in the Milky Way or related to the finite extension of the Local Arm.

Volume filling factor: The presence of the Perseus arm group is probably restricted to the galactic plane and represent only a small subsample. Therefore it is plausible to assume that the majority of the loops with unknown distances belong to the nearby ($D \leq 800$ pc) group. Applying the distance – size distribution obtained for the nearby group to all loops with unknown distances (except the loops of the Perseus group), it is possible to give a rough estimate for the volume filling factor (or porosity Q , Cox & Smith, 1974) of our loop interiors in the galactic disc. Assuming that the loops/bubbles were formed in the cold neutral interstellar medium (justified by their FIR colours) using $z_H = 250$ pc for the scale height of HI (Nakanishi & Sofue, 2003) in the solar neighbourhood, we obtain a volume filling factor of $f_{2nd} \approx 4.6\%$ for the 2nd Galactic Quadrant for $D \leq 800$ pc. Taking into account an additional $\sim 40\%$ of loops in the midplane (see above) an upper limit of $f_{2nd} \approx 6.4\%$ can be obtained. These values confirm the filling factors by Ferrière (1998) and Gazol-Patiño & Passot (1999) ($f = 3\text{--}8\%$ for $8.5 \leq R_\odot \leq 10$ kpc galactocentric distances).

5. Summary and outlook

We summarize the main outcomes of our paper below:

- One fourth of the far-infrared sky was surveyed and 145 loops were identified.
- The loop sample is representative in the Local Arm
- The FIR loops outside the midplane possess $\sim 10\%$ column density excess and a cirrus-like $\Delta I_{60}/\Delta I_{100} \approx 0.25$ ratio
- The midplane loops hold several times denser walls and a far-infrared colour of $\Delta I_{60}/\Delta I_{100} > 0.4$
- Distance estimates are given for 30 loops which trace the cold ISM in the Local Arm and in the Perseus Arm
- We estimated the hot gas volume filling factor to be $4.6\% \leq f_{2nd} < 6.4\%$ in the Local Arm in the 2nd Galactic Quadrant

As a continuation of this study the 1st, 3rd and 4th galactic quadrants are surveyed as well. The complete sample and a comparison with HI distribution will be given in a forthcoming paper.

Acknowledgements. This research was partly supported by the Hungarian Research Fund (OTKA), grants #F-022566 and #T-043773. We are grateful to A. Burkert and B.G. Elmegreen for their valuable comments.

References

- Ábrahám, P., Balázs, L.G., Kun, M., 2000, A&A 354, 645
- Beichman, C., Neugebauer, G., Habing, H.J., Clegg, P.E., Chester, T.J. (eds.), IRAS Catalogues and Atlases Explanatory Supplement, 1988, NASA RP-1190, Vol. 1.
- Blaauw, A., 1991, *OB associations and the fossil record of star formation*, in: The Physics of Star Formation and Early Stellar Evolution, eds. Lada, C.J., Kylafis, N.D., Kluwer, p.125
- Blitz, L., Fich, M., Stark, A.A., 1982, ApJS 49, 183
- Boulanger, F., Pérault, M., 1988, ApJ 300, 964
- Brand, P.W.J.L., Zealey, W.J., 1975, A&A 38, 363
- Braunfurth, E., 1983, A&A 117, 297
- Brinks, E., 1981, A&A 95, L1
- Cappa, C.E., Herbstmeier, U., 2000, AJ 120, 1963
- Cernicharo, J., Bachiller, R., Duvert, G., 1985 A&A 149, 273
- Cox, D.P., Smith, B.W., 1974, ApJ 189, L105
- Crawford, D.L., 1994, PASP 106, 397
- Daigle, A., Joncas, G., Parizeau, M., Miville-Deschênes, M.-A., 2003, PASP 115, 662
- Deul, E.R., den Hartog, R.H., 1990, A&A 229, 362
- Dickey, J.M., Lockman, F.J., 1990, ARA&A 28, 215
- Dutra, C.M., Bica, E., 2002, A&A 383, 631
- Efremov, Y.N., Elmegreen, B.G., Hodge, P.W., 1998, ApJ 501, L163
- Ehlerová, S., Palouš, S., 1996, A&A 313, 478
- Elmegreen, B.G., Lada, C.J., 1977, ApJ 214, 725
- Emerson, J.P., 1988, Formation and Evolution of Low Mass Stars, NATO Advanced Institute (ASI) Series C, Volume 241, Kluwer, Dordrecht, p.193
- ESA, 1997, The Hipparcos and Tycho Catalogues, ESA SP-1200
- Ferrière, K., 1998, ApJ 503, 700
- Fich, M., Blitz, L., Stark, A.A., 1989, ApJ 342, 272
- Garmany, C. D., Stencel, R. E., 1992, A&AS 94, 211
- Gazol-Patiño, A., Passot, Th., 1999, ApJ 518, 748
- Green, D.A., 1994, A Catalogue of Galactic Supernova Remnants, in: Proc. of the IAU Coll. 145, Supernovae and Supernova Remnants, eds. McCray, R., Wang, Z., Cambridge University Press.
- Green, D.A., 2001, 'A Catalogue of Galactic Supernova Remnants (2001 December version)', Mullard Radio Astronomy Observatory, Cavendish Laboratory, Cambridge, UK (available on the Word-Wide-Web at "<http://www.mrao.cam.ac.uk/surveys/snrs/>")
- Hartmann, D., Magnani, L., Thaddeus, P., 1998, ApJ 492, 205
- Heiles, C., 1979, ApJ 229, 533
- Heiles, C., 1980, ApJ 235, 833
- Heiles, C., 1984, ApJS 55, 585
- Heiles, C., 1990, ApJ 354, 483
- Hu, E.M., 1981, ApJ 248, 119
- Humphreys, R.M., 1978, ApJS 38, 309
- Joint IRAS Science Working Group, 1988, Infrared Astronomical Satellite Catalogues, The Point Source Catalogue, version 2.0, NASA RP-1190
- Kim, S., Staveley-Smith, L., Dopita, M.A., et al., 1998, ApJ 503, 67
- Kim, S., Staveley-Smith, L., Dopita, M.A., et al., 2003, ApJSS 148, 473
- Kiss, Cs., Moór A., Tóth L.V., et al., 2000, A&A 363, 755
- Klessen, R.S., Hietsch F., Mac Low M.M., 2000, ApJ 535, 887
- Koo, B.-C., Heiles, C., 1991, ApJ 382, 204
- Koo, B.-C., Heiles, C., Reach, W.T., 1992, ApJ 390, 108
- Korpi, M.J., Brandenburg, A., Shukorov, A., Tuominen, I., 1999, A&A 350, 230
- Krügel, E., 2003, The Physics of Interstellar Dust, Institute of Physics Publishing, Bristol and Philadelphia
- Kun, M., Balazs, L.G., Toth, I., 1987, Ap&SS 134, 211
- Kun, M., 1998, ApJS 115, 59
- Lagache, G., Abergel, A., Boulanger, F., Désert, F.X., Puget, J.-L., 1999, A&A 344, 322
- Lang, K.R., 1992, Astrophysical Data: Planets and Stars, Springer, Heidelberg
- Large, M.I., Quigley, M.J.S., Haslam, C.G.T., 1962, MNRAS 124, 405
- Large, M.I., Quigley, M.J.S., Haslam, C.G.T., 1966, MNRAS 131, 335
- Loeb, A., Perna, R., 1998, ApJ 503, L35
- Low, F., Beintema, D.A., Gautier, F.N., et al., 1984, ApJ 278, L19
- Magnani, L., Hartmann, D., Holcomb, S.L., Smith, L.E., Thaddeus, P., 2000, ApJ 535, 167
- Marston, A.P., 1996, AJ 112, 2828
- McKee, C.F., Ostriker, J.P., 1977, ApJ 218, 148
- Meyerdierks, H., Heithausen, A., Reif, K., 1991, A&A 245, 247
- Meyerdierks, H., 1991, A&A 251, 269
- Moór, A., Kiss, Cs., 2003, *Multiwavelength study of the CasOB5 supershell*, in: The Interaction of Stars With Their Environment II., eds. Kiss, Cs., et al, CoKon 103, 149
- Nakanishi, H., Sofue, Y., 2003, PASJ 55, 191
- Obayashi, A., Kun, M., Sato, F., Yonekura, Y., Fukui, Y., 1998, AJ 115, 274
- Oey, M.S., Clarke, C.J., 1997, MNRAS 289, 570
- Oort, J.H., 1954, Bull. Astron. Inst. Neth. 12, 177
- Öpik, E.J., 1953, Irish Astron. J. 2, 219
- Palouš, J., Franco, J., Tenorio-Tagle, G., 1990, A&A 227, 175
- Palouš, J., 1996, *How does star formation affect the large scale structure of the ISM?*, in: Unresolved Problems of the Milky Way, eds. Blitz, L., Teuben, P., IAU Symposium #169, p.583
- Pfeffermann, E., Achenbach, B., Predehl, P., 1991, A&A 246, L28
- Pound, M.W., Goodman, A.A., 1997, ApJ 482, 334
- Sánchez-Salcedo, F.J., 2001, ApJ 563, 867
- Schlegel, D.J., Finkbeiner, D.P., Davis, M., 1998, ApJ 500, 525
- Schwartz, P.R., 1987, ApJ 320, 258
- Sharpless, S., 1959, ApJS 4, 257
- Staveley-Smith, L., Davies, R.D., Kinman, T.D., 1992, MNRAS 258, 334
- Taylor, J.H., Manchester, R.N., Lyne, A.G., 1993, ApJS 88, 529
- Tenorio-Tagle, G., Bodenheimer, P., 1988, ARA&A 26, 145
- Ungerechts, H., Thaddeus, P., 1987, ApJS 63, 645
- Uyaniker, B., Landecker, T.L., 2002, ApJ 575, 225

Wada, K., Spaans, M., Kim, S., 2000, ApJ 540, 797

Wheelock, S.L., Gautier, T.N., Chillemi, J., et al., 1994, IRAS

Sky Survey Atlas Explanatory Supplement, JPL Publ. 94-11

de Zeeuw, P.T., Hoogerwerf, R., de Bruijne, J.H.J., Brown, A.G

A., Blaauw, A., 1999, AJ 117, 354

Appendix A, B and C are available at the following URL: "<http://astro.elte.hu/CFIRLG>" as single PostScript files.